Int. J. Multiphase Flow Vol. 14, No. 2, pp. 203–215, 1988
Printed in Great Britain

0301-9322/88 $3.00 + 0.00
Pergamon Press/Elsevier

RADIAL PENETRATION OF A VISCOUS LIQUID INTO A PLANAR ANISOTROPIC POROUS MEDIUM

K. L. ADAMS, W. B. RUSSEL and L. REBENFELD
Textile Research Institute and Department of Chemical Engineering, Princeton University, Princeton, NJ 08544, U.S.A.

(*Received* 28 *May* 1987; *in revised form* 1 *November* 1987)

Abstract—The equations describing the radial encroachment of a viscous liquid into a homogeneous, anisotropic porous medium are formulated and solved by two approximate methods. An analytical approximation is in good agreement with a finite element numerical solution, provided the angular component of the pressure gradient in an elliptical coordinate system is small. In the specific case where one of the principal flow directions is perpendicular to the flow plane, treatment of experimental flow data in accord with the analytical approximation determines the principal in-plane permeabilities and the degree of in-plane anisotropy. In the general case, the analysis yields effective permeabilities that are functions of the principal permeabilities and the orientation of the principal coordinate system.

INTRODUCTION

A porous medium is anisotropic with respect to fluid flow if the directions of the superficial fluid velocity and the imposed pressure gradient generally differ. Then the permeability, as defined for inertialess flows by Darcy's law, is directionally dependent. Anisotropy is distinct from the spatial variation of permeability caused by nonuniformities or heterogeneities. Examples of anisotropic media include naturally occurring oil sands and rock formations and fabricated materials such as textiles. Flow anisotropies in these materials reflect structural anisotropies. Preferred grain orientation in geological formations is responsible for the directional variation in flow resistance. Similarly, preferred fiber orientation in nonwoven fabrics and constructional characteristics of woven and knit fabrics are the major structural anisotropies of these materials.

The fluid flow conductance of an anisotropic medium is described in terms of a permeability tensor, $\mathbf{k}$, which relates components of the fluid velocity to components of the pressure gradient. Diagonalization of this tensor, assumed symmetric, defines the principal flow directions of the medium, characterized by the principal permeabilities, k_1, k_2 and k_3. Often, a porous medium is only two-dimensionally anisotropic and two permeabilities suffice. For example, the idealized case of a linear fibrous network comprised of infinitely long parallel circular cylinders is characterized by a permeability parallel to the cylinder axis and a single permeability in the perpendicular direction (e.g. Neale 1977).

Anisotropic permeabilities are quantified by measuring components of the pressure drop and superficial velocity in one or more flow directions. Usually, one of the principal flow directions is assigned by physical arguments before the experiments are performed. The direction perpendicular to the bedding plane of an oil sandstone or a planar fibrous material is typically considered as one of the three principal flow directions. In these cases, experiments are usually limited to quantifying the permeability transverse to the plane and to identifying the in-plane principal flow directions and permeabilities. Clearly, the in-plane principal permeability determinations present the most difficulty because the in-plane principal flow directions are not known.

Steady, unsteady and pseudo-steady-state methods have been developed to measure directional permeabilities (e.g. Rice *et al.* 1970; Bear 1972). In the majority of cases, the flow geometry is linear and allows only a single directional measurement on a given test specimen. A new test specimen must be cut or the sample rotated to test other directions. Rose (1982) presented a one-dimensional flow technique that requires just two test specimens to quantify two-dimensional principal flow directions and permeabilities. In this method, the endface angles of two cylindrical core specimens are altered in a trial-and-error manner until all streamlines are parallel to the core axes and all equipotential surfaces are parallel to the endfaces. The angles that the endfaces make with the core axis define the principal flow directions and allow calculation of the principal permeabilities. Although requiring only two test specimens, the method generally requires more than two flow measurements.

Only a few permeability measuring methods have used two-dimensional flows. Johnson & Hughes (1948) developed a two-dimensional radial flow apparatus which utilized a single hollowed cylindrical test specimen. Gas flowed radially under a fixed driving pressure from the hollowed core to the outer radius of the specimen. There, a moveable gas collection head determined the volumetric flow rate as function of in-plane angle. Fontugne (1969) measured the principal permeabilities of unconsolidated porous media in a rectangular flow cell by matching the ratio of horizontal and vertical flows with a numerical solution of the governing equations.

The superficial velocity and pressure gradient vectors are collinear only in the principal flow directions. In these directions the permeability is unique and equal to one of the principal permeabilities. In directions other than the principal flow directions, the permeabilities are not simply related to components of the permeability tensor (Scheidegger 1960; Marcus 1962; Dullien 1979). In the absence of a consistent theory, directional permeability data are typically plotted as $k^{1/2}$ or $k^{-1/2}$ vs in-plane angle and statistically fit to an ellipse. The semimajor and semiminor axes of the ellipse define the principal flow directions.

Although straightforward in their application, the methods presented to date to measure directional permeabilities have been hindered by several common problems. The most severe problem is the large number of individual measurements and specimens required to uniquely quantify the directional permeabilities and the principal flow directions, even for two-dimensional anisotropies. Also, many of the experimental systems, especially the one-dimensional linear flows are subject to channelling and boundary effects. Finally, if nonuniformities are present in the system, there is no simple way to determine whether the variation in directional permeability is due to pure anisotropy or to nonuniformities and heterogeneities (Greenkorn *et al.* 1964).

Recently, we demonstrated the feasibility of monitoring the radial encroachment of a viscous liquid into a planar porous medium (Adams *et al.* 1986). In this situation, the in-plane anisotropy dictates the shape of the advancing fluid front and the directional permeabilities determine the rate of penetration for a given driving pressure and fluid viscosity. In this paper, we derive the equations which predict the radial advancement of a fluid into a planar porous medium under pseudo-steady-state flow conditions. Using these equations, we show how to define directional in-plane permeabilities and the directions of the principal axes from a single experiment on a single test specimen.

THEORY

The radial penetration of liquid into a homogeneous, anisotropic porous medium is depicted in figure 1. At $t = 0$, liquid begins entering the porous material from a cylindrical boundary of radius R_0 at pressure P_0. At a later time, t, the moving front resembles an ellipse characterized by maximum and minimum radial extents. R_{f1} and R_{f2}, and orientation, θ, relative to a laboratory coordinate system. The pressure at the moving front is P_f. The characteristic properties of the medium are the porosity, ϵ, and the thickness, h, which is large enough to neglect any flow resistance due to the boundaries, yet small enough to minimize gravitational effects. The spreading process is considered pseudo-steady if the process time scale is large with respect to the microscopic time scale for momentum transfer (Whitaker 1970) and the time scale of compressibility effects (Greenkorn 1983). Since the displaced fluid is air, the interface is unconditionally stable due to a favorable viscosity ratio and flow direction (Wilson 1975; Paterson 1981). Although a finite surface tension exists at the flow front, surface wettability forces are assumed small in comparison to the external driving force.

The equations describing the fluid motion are the continuity equation for incompressible flow,

$$\nabla \cdot \mathbf{v}_0 = 0 \qquad [1]$$

and the tensorial form of Darcy's law,

$$\mathbf{v}_0 = \frac{-\mathbf{k} \cdot \nabla P}{\mu}; \qquad [2]$$

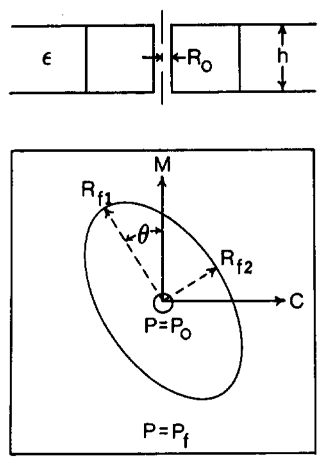

Figure 1. Radial penetration of liquid into a homogeneous, anisotropic porous medium.

$\mathbf{v}_0$ is the superficial velocity vector and μ is the viscosity of the penetrating liquid. If one of the principal flow directions is perpendicular to the flow plane, combining [1] and [2] in a coordinate system, (x_1, x_2), corresponding to the in-plane principal flow directions, gives

$$\frac{\partial^2 P}{\partial x_1^2} + \alpha \frac{\partial^2 P}{\partial x_2^2} = 0. \quad [3]$$

Principal permeabilities, k_1 and k_2, determine $\alpha = k_2/k_1$, the in-plane degree of anisotropy.

For a principal coordinate system with arbitrary orientation with respect to the flow plane, [3] is still valid provided directions 1 and 2 are identified as effective principal flow directions with permeabilities k_1^{eff} and k_2^{eff} and $h/R_f \ll 1$ to ensure a nearly uniform flow cross-section. The effective permeabilities are functions of the principal permeabilities and the orientation of the principal coordinate system:

$$k_1^{\text{eff}} = k_1 l_1^2 + k_2 m_1^2 + k_3 n_1^2 \quad [4]$$

and

$$k_2^{\text{eff}} = k_1 l_2^2 + k_2 m_2^2 + k_3 n_2^2. \quad [5]$$

In these equations, l_i, m_i and n_i are the direction cosines of principal flow directions 1, 2 and 3 with the ith direction of the in-plane coordinate system.

The boundary conditions associated with [3] are

$$P = P_0 \quad \text{at} \quad x_1^2 + x_2^2 = R_0^2 \quad [6]$$

$$P = P_f \quad \text{at} \quad R_f(x_1, x_2, t). \quad [7]$$

Furthermore, a kinematic condition imposed at the moving front requires that the boundary propagate with the local fluid velocity

$$\mathbf{v}_f = \frac{d\mathbf{x}_f}{dt} = \frac{\mathbf{v}_0}{\epsilon}\bigg|_{R_f}. \quad [8]$$

Solving [3] for the pressure distribution, substituting the distribution into [2] and evaluating this equation at the moving front determines the superficial frontal velocity vector. Substitution into [8] generates the differential equations which predict the time evolution of the advancing liquid front.

Moving boundary problems of this type require that the shape of the interface be known from symmetry conditions or be obtained as part of the solution. If the problem is linearly, radially or spherically symmetric, an exact, analytic solution is possible. In most other cases, numerical techniques or analytic approximations are required (Wilson *et al.* 1978).

ISOTROPIC SOLUTION

The radially symmetric case of this analysis occurs when $k_2 = k_1 = k$, i.e. the porous medium is isotropic within the plane. Then the fluid front is macroscopically circular and the pressure varies only radially according to

$$\frac{P - P_f}{P_0 - P_f} = \frac{P - P_f}{\Delta P} = 1 - \frac{\ln\left(\frac{R}{R_0}\right)}{\ln\left(\frac{R_f}{R_0}\right)}. \qquad [9]$$

The radial component of the superficial velocity vector evaluated at $R = R_f$ gives

$$v_{0r}|_{R_f} = \frac{k\Delta P}{\mu} \frac{1}{R_f \ln\left(\frac{R_f}{R_0}\right)}. \qquad [10]$$

The differential equation generated by the kinematic condition is

$$\frac{dR_f}{dt} = \frac{k\Delta P}{\epsilon\mu} \frac{1}{R_f \ln\left(\frac{R_f}{R_0}\right)} \qquad [11]$$

with the initial condition

$$R_f = R_0 \quad \text{at} \quad t = 0. \qquad [12]$$

The dimensionless solution of [11] and [12] is

$$\rho_f^2(2 \ln \rho_f - 1) + 1 = 4\Phi, \qquad [13]$$

where $\rho_f = R_f/R_0$ is the dimensionless radial extent and $\Phi = k\Delta Pt/\epsilon\mu R_0^2$ is a dimensionless time which fully accounts for the experimental variables in the system. Equation [13] predicts the radial encroachment of a liquid into a homogeneous, isotropic porous medium.

ANISOTROPIC SOLUTION

When $k_2 \neq k_1$, the porous medium is anisotropic within the plane and the shape of the flow front is not evident from the problem geometry. Prior to an approximate solution, it is useful to transform [3] to Laplace's equation by scaling as (Kucuk & Brigham 1979; Greenkorn 1983)

$$x_1' = x_1\alpha^{1/4}, \qquad [14]$$

$$x_2' = x_2\alpha^{-1/4} \qquad [15]$$

and

$$P' = \frac{P - P_f}{\Delta P}, \qquad [16]$$

to obtain

$$\frac{\partial^2 P'}{\partial x_1'^2} + \frac{\partial^2 P'}{\partial x_2'^2} = 0 \qquad [17]$$

with the boundary conditions

$$P' = 1 \quad \text{at} \quad \frac{x_1'^2}{\alpha^{1/2}} + \frac{x_2'^2}{\alpha^{-1/2}} = R_0^2 \qquad [18]$$

and

$$P' = 0 \quad \text{at} \quad R_f'(x_1', x_2', t). \qquad [19]$$

Physically, this scaling has shifted the anisotropy of the problem to the geometry of the inlet hole. Flow from a circular boundary into an anisotropic medium has been transformed into flow from an elliptical boundary into an isotropic medium of permeability $\bar{k} = (k_1 k_2)^{1/2}$. The semimajor and semiminor axes of the inlet hole are $R_0\alpha^{-1/4}$ and $R_0\alpha^{1/4}$, respectively, so that as $\alpha \to 1$ the inlet hole returns to a circle.

Since the inner boundary is an ellipse, an elliptical coordinate system is natural for attempting a solution. The relationship between elliptical coordinates ξ and η and rectangular coordinates x_1' and x_2' is (figure 2)

$$x_1' = L \sinh \xi \sin \eta \qquad [20]$$

and

$$x_2' = L \cosh \xi \cos \eta, \qquad [21]$$

where L is one half the focal length of the entrance ellipse, i.e.

$$L = R_0(\alpha^{-1/2} - \alpha^{1/2})^{1/2}. \qquad [22]$$

Lines of constant ξ and η form families of confocal ellipses and hyperbolas, respectively. In this coordinate system, [17]–[19] become

$$\frac{\partial^2 P'}{\partial \xi^2} + \frac{\partial^2 P'}{\partial \eta^2} = 0 \qquad [23]$$

$$P' = 1 \quad \text{at} \quad \xi = \xi_0 \qquad [24]$$

and

$$P' = 0 \quad \text{at} \quad R_f'(\xi, \eta, t), \qquad [25]$$

respectively. The elliptical equivalent of the inlet boundary, ξ_0, is only a function of α given by

$$\xi_0 = \ln\left[\frac{1 + \alpha^{1/2}}{(1-\alpha)^{1/2}}\right]. \qquad [26]$$

Darcy's law in elliptical coordinates is

$$\mathbf{v}_0 = \mathbf{i}_\xi v_{0\xi} + \mathbf{i}_\eta v_{0\eta} = \frac{-\bar{k}\Delta P}{\mu}\nabla P' = \frac{-\bar{k}\Delta P}{\mu}\left[\frac{1}{L(\cosh^2\xi - \cos^2\eta)^{1/2}}\left(\mathbf{i}_\xi \frac{\partial P'}{\partial \xi} + \mathbf{i}_\eta \frac{\partial P'}{\partial \eta}\right)\right], \qquad [27]$$

where $\mathbf{i}_\xi$ and $\mathbf{i}_\eta$ are unit vectors in the ξ and η directions, respectively. Furthermore, the kinematic condition at the moving boundary becomes

$$\mathbf{v}_f = L(\cosh^2\xi_f - \cos^2\eta_f)^{1/2}\left(\mathbf{i}_\xi \frac{d\xi_f}{dt} + \mathbf{i}_\eta \frac{d\eta_f}{dt}\right). \qquad [28]$$

The governing anisotropic flow equations have been scaled to shift the anisotropic effects from the pressure equation to a boundary condition, and a subsequent coordinate transformation has placed the problem in a natural elliptical coordinate system. Equations [23]–[25] coupled with [27] and [28] are now solved by two approximate methods.

Numerical solution

In problems involving geometrically irregular boundaries, the finite element numerical technique is widely used. With respect to flow in porous media, this method is routinely applied to moving boundary problems in subsurface hydrology and petroleum engineering (e.g. Conner & Brebbia 1976; Pinder & Gray 1977). Generally, the problem is solved by considering the transient solution to be a sequence of steady-state solutions separated by small time increments. After solving the problem for an initial boundary condition, pressure gradients at the interface are evaluated and used to propagate the interface to the next time step. The propagation step may be explicit in the current boundary or implicit, requiring iteration to find the new boundary. The procedure of solving a steady-state problem and propagating the interface is continued until a specified time is reached or steady conditions prevail.

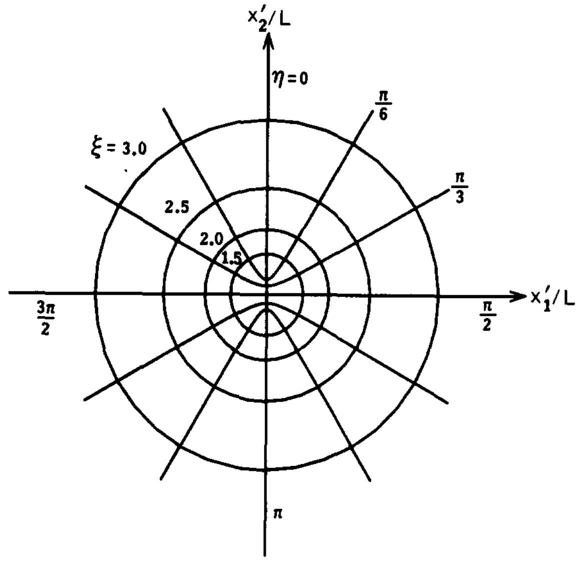

Figure 2. Elliptical coordinate system.

Galerkin's method of weighted residuals was used to obtain a numerical solution to the anisotropic flow problem. Triangular elements with linear basis functions covered the solution domain, $0 < \eta < \pi/2$ and $\xi_0 < \xi < \xi_f(\eta)$. To take advantage of problem symmetry only a quarter of the full domain was used with the $\partial P'/\partial\eta = 0$ symmetry condition at $\eta = 0$ and $\eta = \pi/2$. Nodal pressures were determined through a stationary, linear iteration of the Gauss–Seidel type. With the pressure distribution of the previous time step as an initial guess to the iteration procedure, the solution of the system of equations always converged within 10 iterations to a nodal pressure accuracy of 10^{-5}. Forward difference approximations for the derivatives in [28] were used to advance the liquid front with three different dimensionless time increments, $\Delta\Phi$, to reflect the variation of interfacial pressure gradients encountered. Near the inlet hole, where $0 < \Phi < 0.1$ and the pressure gradient is the largest, the time increment was 0.001. In the intermediate region, $0.1 < \Phi < 1.0$, and the remainder, $\Phi > 1.0$, the time increments were 0.01 and 0.05, respectively. Fronts were propagated until $\Phi = 100$. In all cases, Φ is defined as in the isotropic solution, but based on k_1, the maximum in-plane principal permeability.

Numerical solutions were obtained for α in the range 0.1–0.9. For all degrees of anisotropy considered, the solution domain was discretized into 80 elements and 54 nodes. For $\alpha = 0.1$, 16 element, 15 node and 162 element, 100 node solutions were also calculated to evaluate the accuracy of the solution.

Table 1 shows numerical data obtained for $\alpha = 0.1$ and the three different mesh configurations. The results are presented as frontal elliptical and dimensionless radial extents in the principal flow

Table 1. Convergence of a finite element solution, $\alpha = 0.1$

Φ	N	ξ_{f1}	ξ_{f2}	ρ_{f1}	ρ_{f2}
1	15	0.7267	0.9083	2.377	1.368
	54	0.7276	0.9043	2.380	1.364
	100	0.7279	0.9029	2.382	1.362
10	15	1.290	1.413	5.036	2.064
	54	1.295	1.407	5.066	2.053
	100	1.297	1.405	5.077	2.049
50	15	1.834	1.896	9.149	3.230
	54	1.839	1.891	9.197	3.214
	100	1.841	1.889	9.216	3.208
100	15	2.090	2.133	11.94	4.060
	54	2.094	2.129	11.99	4.044
	100	2.096	2.127	12.01	4.036

directions. Because the change in the solution as the number of nodes and elements is increased is small, further mesh refinements are unwarranted and 54 node solutions are presented for further analysis.

Contour plots for $\alpha = 0.9$, 0.5 and 0.1 are shown in figure 3. As α decreases, there is a significant increase in the eccentricity of the fluid front. For a given dimensionless time, changes in the radial extent of principal direction 1 with degree of anisotropy are slight, while there are large changes in the radial extent of principal direction 2. Plotted as ρ_{f1} and ρ_{f2} vs Φ in figure 4, the same effect is evident. Deviations of the ρ_{f2} curves from the in-plane isotropic case, $\alpha = 1.0$, are much smaller than the corresponding deviations of ρ_{f1}. As expected, the rate of movement of the fluid front is initially high then decreases monotonically as more of the porous medium is filled and the resistance to fluid flow is increased. The results of these numerical solutions show that the shape of the advancing fluid front is a sensitive indicator of the degree of in-plane anisotropy and that the absolute rate of fluid movement is determined by the combination of variables that form Φ.

Since the anisotropic problem was solved in its natural coordinate system, one might expect that the η-dependence of the moving boundary would be small. Indeed, the data in table 1 reveal large differences between ρ_{f1} and ρ_{f2} for a given Φ but much smaller differences between ξ_{f1} and ξ_{f2}, particularly for large Φ. To assess the relative contributions of driving pressure in the ξ and η directions, the maximum value of $|\partial P'/\partial \eta|/|\partial P'/\partial \xi|$ at the moving boundary was determined as part of the solution. The location of the maximum ratio varied with α and was a finite distance from the inlet hole. As shown in figure 5, the maximum ratio increases as α becomes small, indicating that more η-dependence is introduced as the anisotropy increases, In all cases, however, the ratio is <0.1.

Analytical approximation

If the η-component of the pressure gradient in the governing equations is neglected, the equations are reduced to form that has an analytical solution. We know that the solution will have the correct zero-time limit and we expect that it will also have the correct long-time limit as details of the inlet hole shape become unimportant at long distances. In the long-time limit, the fluid front is elliptical and the pressure distribution reduces to

$$P'(\xi) = \frac{\xi_f - \xi}{\xi_f - \xi_0}. \tag{29}$$

Therefore, the pressure gradient driving the flow is constant throughout the fluid at

$$\frac{dP'}{d\xi} = \frac{-1}{\xi_f - \xi_0}. \tag{30}$$

Using [29] and [30] as the basis for the approximation, [27] gives the approximate superficial fluid velocity at the interface,

$$v_{0\xi}|_{\xi_f} = \frac{\bar{k}\Delta P}{\mu L(\cosh^2\xi_f - \cos^2\eta)^{1/2}}\frac{1}{(\xi_f - \xi_0)}. \tag{31}$$

The η-dependence of the superficial fluid velocity simply indicates that the solution is not exact. Combining [31] with the kinematic boundary condition, [28], yields a dimensionless differential equation predicting the time evolution of the moving boundary:

$$\frac{d\xi_f}{d\Phi} = \left(\frac{\alpha}{1-\alpha}\right)\left[\frac{1}{(\xi_f - \xi_0)(\cosh^2\xi_f - \cos^2\eta)}\right], \tag{32}$$

with the initial condition

$$\xi_f = \xi_0 \quad \text{at} \quad \Phi = 0. \tag{33}$$

The solution is

$$F(\xi_f, \eta) = (\xi_f - \xi_0)\left[\frac{\sinh(2\xi_f)}{4} + \frac{\xi_f}{2}\right] - \frac{\cos^2\eta\,(\xi_f - \xi_0)^2}{2} + \frac{[\cosh(2\xi_0) - \cosh(2\xi_f)]}{8} + \frac{(\xi_0^2 - \xi_f^2)}{4} = \left(\frac{\alpha}{1-\alpha}\right)\Phi. \tag{34}$$

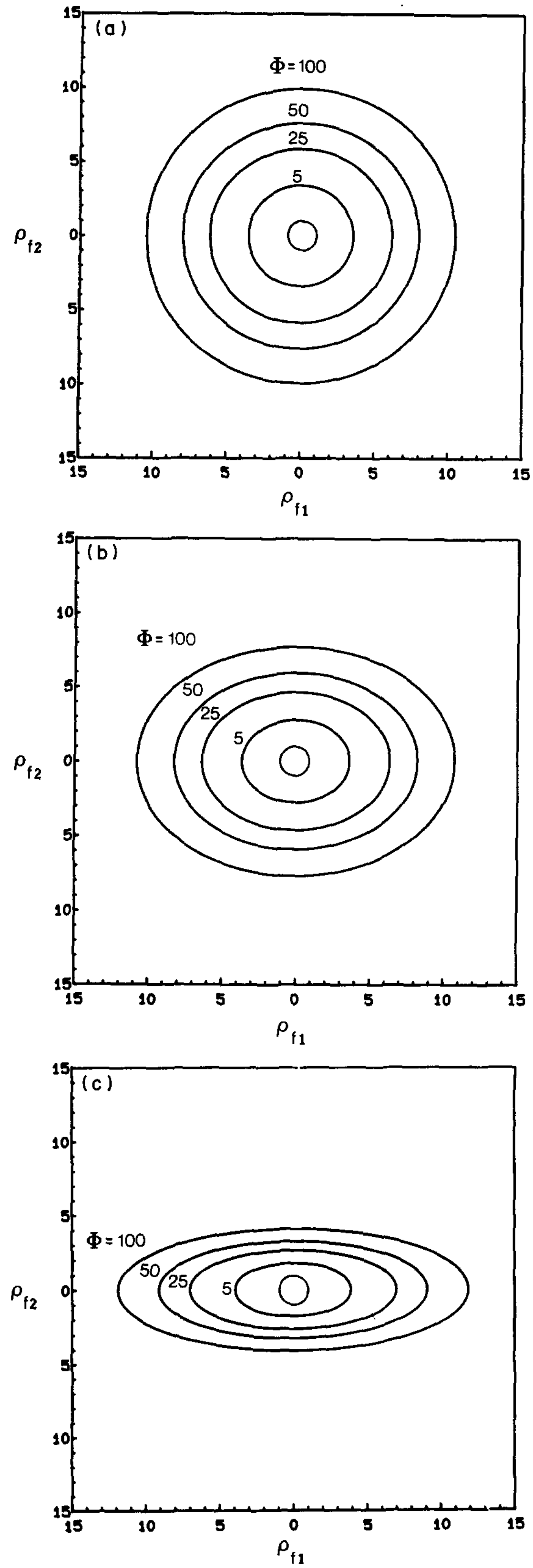

Figure 3. Radial flow contour plots for: (a) $\alpha = 0.9$; (b) $\alpha = 0.5$; (c) $\alpha = 0.1$.

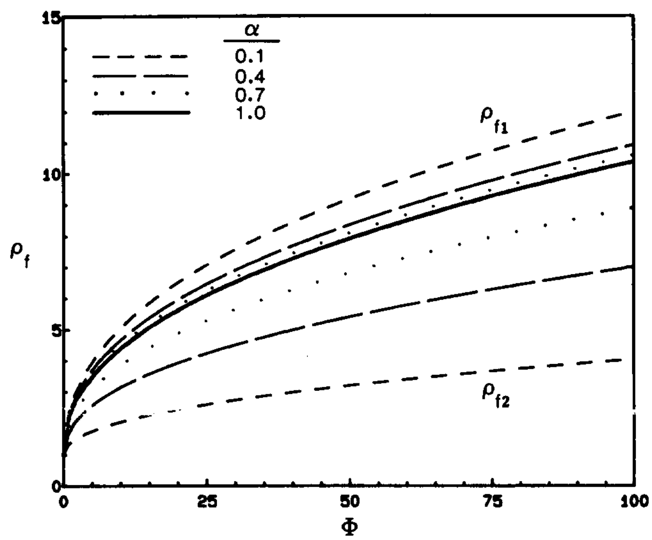

Figure 4. Φ-dependence of dimensionless principal flow direction radial extents.

In the limit of long times, ξ_f becomes large compared to ξ_0 and the hyperbolic terms of [34] become dominant and yield the long-time asymptote,

$$\frac{\xi_f \sinh(2\xi_f)}{4} = \left(\frac{\alpha}{1-\alpha}\right)\Phi. \quad [35]$$

As evidenced by [35], the flow front at long times is elliptical and independent of inlet hole shape (ξ_0). In-plane anisotropy serves only to modify the time required to reach a given shape.

Comparison of solutions

Table 2 compares the 54 node finite element solution with the analytic approximation given by [34]. The error associated with the approximation is $<1\%$ for the range of anisotropies considered and decreases as α increases. The close correspondence between the solutions is readily apparent in figure 6, where the solutions are plotted for $\alpha = 0.1$, the largest anisotropy considered. The analytic approximation slightly underpredicts the maximum radial extent and overpredicts the minimum radial extent.

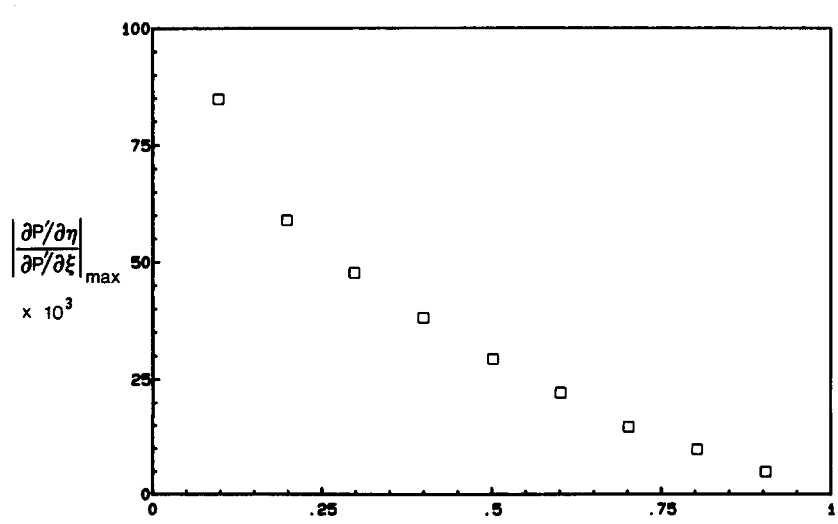

Figure 5. Ratio of pressure gradient components as a function of degree of anisotropy.

Table 2. Comparison of a finite element solution with an analytic approximation

α	Φ	ξ_{f1} $N=54$	ξ_{f1} Equation [34]	%Diff.	ξ_{f2} $N=54$	ξ_{f2} Equation [34]	%Diff.
0.1	1	0.7276	0.7246	0.41	0.9043	0.9122	0.87
	10	1.295	1.284	0.85	1.407	1.420	0.92
	50	1.839	1.828	0.60	1.891	1.902	0.58
	100	2.094	2.086	0.38	2.129	2.138	0.42
0.5	1	1.565	1.562	0.12	1.620	1.621	0.06
	10	2.235	2.230	0.22	2.258	2.261	0.13
	50	2.809	2.806	0.11	2.818	2.820	0.07
	100	3.074	3.072	0.06	3.080	3.081	0.03
0.9	1	2.605	2.603	0.08	2.612	2.611	0.04
	10	3.290	3.288	0.06	3.293	3.292	0.03
	50	3.872	3.871	0.03	3.873	3.872	0.03
	100	4.140	4.139	0.02	4.141	4.140	0.02

The error in the approximation appears to go through a maximum at some position away from the inlet hole, consistent with the η-dependence generated by the analytic approximation.

$$\left.\frac{d\xi_f}{d\eta}\right|_{\Phi},$$

obtained from [34],

$$\left.\frac{d\xi_f}{d\eta}\right|_{\Phi} = \frac{\cos\eta\,\sin\eta\,(\xi_0-\xi_f)}{\cosh^2\xi_f-\cos^2\eta}, \tag{36}$$

is identically zero at the inlet boundary where $\xi_f=\xi_0$ and, consistent with the long-time asymptote, tends to zero as ξ_f becomes large. The frontal position associated with the maximum value of this derivative roughly corresponds with the position of the maximum error in the analytic approximation.

APPLICATION

Since the analytic solution represents a good approximation over the range of anisotropies considered, it may be used to determine directional permeabilities from a radial encroachment experiment. While it is also possible to use the more accurate long-time asymptote in the analysis, it is not experimentally practical due to the need for large samples and long flow times.

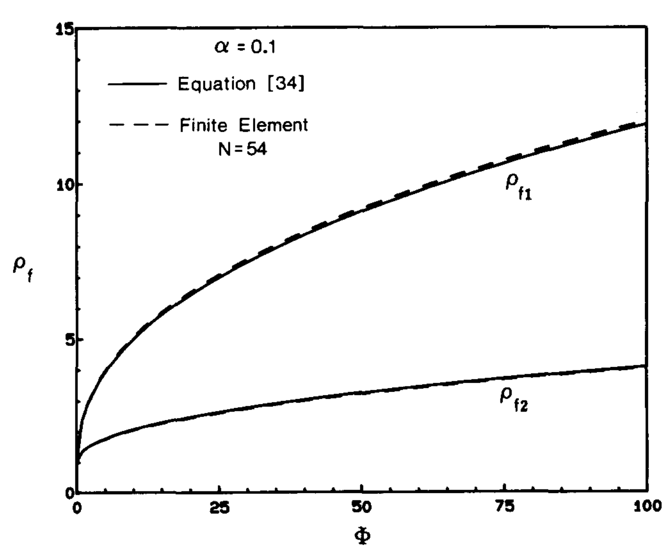

Figure 6. Comparison of a finite element solution ($N=54$) with an analytic approximation, [34], for $\alpha=0.1$.

For nearly elliptical flow fronts, experimental data are easily gathered in the principal flow directions as $R_{f1}(t)$ and $R_{f2}(t)$ (Adams *et al.* 1986). The analysis is iterative in the degree of anisotropy. First α is guessed and R_{f1} and R_{f2} data are converted to equivalent elliptical extents, ξ_{f1} and ξ_{f2}, using

$$\xi_{f1} = \sinh^{-1}\left[\frac{R_{f1}}{R_0}\left(\frac{1}{\alpha} - 1\right)^{-1/2}\right] \quad [37]$$

and

$$\xi_{f2} = \cosh^{-1}\left[\frac{R_{f2}}{R_0}(1-\alpha)^{-1/2}\right]. \quad [38]$$

Subsequently, the l.h.s. of [34], $F(\xi_f, \eta)$, is evaluated for each elliptical extent, using $\eta = \pi/2$ and $\eta = 0$ for principal directions 1 and 2, respectively. The data are then plotted as $F(\xi_f, \eta)$ vs t and the best-fit line obtained. If α is not chosen correctly, the data will not correlate well with the least-squares line. The optimum α minimizes the square of the deviations of the data from the best-fit line. The square of the deviations is unimodal in α and the search procedure is conveniently performed on a microcomputer. When the minimum is located, the slope of the best-fit line,

$$m_\xi = \frac{k_1 \Delta P}{\epsilon \mu R_0^2}\left(\frac{\alpha}{1-\alpha}\right), \quad [39]$$

yields k_1 and k_2 provided that the driving pressure, porosity and fluid viscosity are known. If k_1 and k_2 are the effective permeabilities defined by [4] and [5], the orientation of the principal coordinate system with respect to the in-plane coordinate system and one of the principal permeabilities must be known to quantify the other two principal permeabilities.

As an example of the analysis, consider the anisotropic flow data of a typical screening fabric given in Table 3. Structural properties of the fabric and details of the data acquisition are given elsewhere (Adams & Rebenfeld 1987). The α which minimized the square of the deviations was 0.740, yielding a correlation coefficient >0.99. Figure 7 illustrates the corresponding anisotropic data plot.

CONCLUSION

The radial encroachment of a liquid into a homogeneous, planar porous medium can be described by an approximate analytic solution to the equations describing the flow process provided

Table 3. Experimental data for an anisotropic screening fabric

$t(s)$	ρ_{f1}	$\xi_{f1}(\alpha = 0.74)$	$F(\xi_{f1}, \pi/2)$
	Principal direction 1		
0	2.0	1.93	1.7
55	3.0	2.33	8.0
150	4.0	2.61	20.0
318	5.0	2.83	38.6
522	6.0	3.01	64.3
768	7.0	3.17	97.8
1104	8.0	3.30	139.4
	Principal direction 2		
$t(s)$	ρ_{f2}	$\xi_{f2}(\alpha = 0.74)$	$F(\xi_{f2}, 0)$
13	2.0	2.04	2.6
105	3.0	2.46	11.8
250	4.0	2.75	29.5
471	5.0	2.97	56.6
768	6.0	3.16	94.1
1140	7.0	3.31	142.6
1548	8.0	3.45	202.8

$\Delta P = 2.0 \times 10^4$ Pa; $\mu = 14.5$ Pa·s; $R_0 = 5.0 \times 10^{-3}$ m; $\epsilon = 0.647$; $\alpha = 0.740$; $m_\xi = 0.128\ s^{-1}$; $r = 0.999$; $k_1 = 5.27 \times 10^{-10}\ m^2$ (534 darcy); $k_2 = 3.90 \times 10^{-10}\ m^2$ (395 darcy).

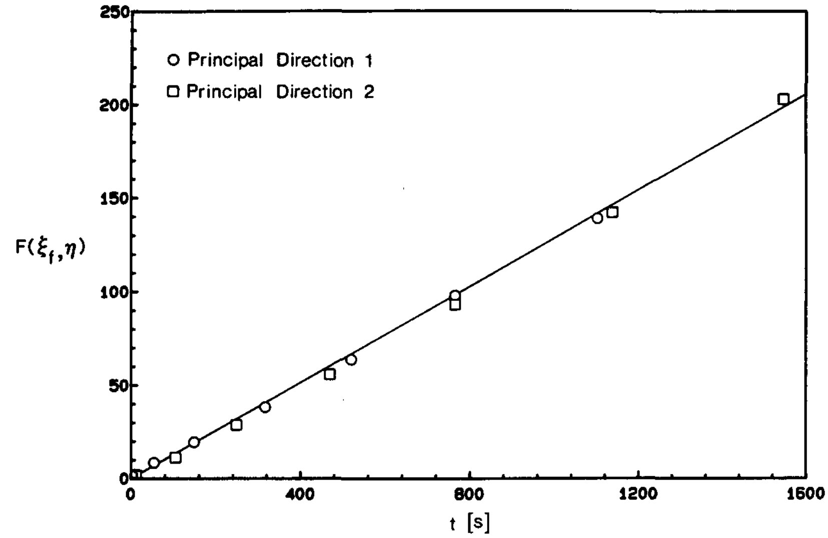

Figure 7. Example anisotropic data plot.

the angular component of the pressure gradient in an elliptical coordinate system is small. If one of the principal flow directions is perpendicular to the flow plane, the principal in-plane permeabilities and the degree of in-plane anisotropy are extracted from frontal movement in the two principal flow directions by analyzing experimental data in accordance with the approximate solution. If the direction perpendicular to the flow plane is not a principal flow direction, the analysis yields effective permeabilities that are functions of the principal permeabilities and the orientation of the principal coordinate system. This technique to measure permeabilities requires just a single test specimen and a single, well-characterized experiment.

REFERENCES

ADAMS, K. L. & REBENFELD, L. 1987 In-plane flow of fluids in fabrics: structure/flow characterization. *Textile Res. J.* **57**, 647–654.

ADAMS, K. L., MILLER, B. & REBENFELD, L. 1986 Forced in-plane flow of an epoxy resin in fibrous networks. *Polym. Engng Sci.* **26**, 1431–1441.

BEAR, J. 1972 *Dynamics of Fluids in Porous Media.* Elsevier, New York.

CONNER, J. J. & BREBBIA, C. A. 1976 *Finite Element Techniques for Fluid Flow.* Newnes-Butterworths, London.

DULLIEN, F. A. L. 1979 *Porous Media: Fluid Transport and Pore Structure.* Academic Press, New York.

FONTUGNE, D. 1969 Permeability measurement in anisotropic media. M. S. Thesis, Dept of Chemical Engineering and Metallurgy, Syracuse Univ., Syracuse, N.Y.

GREENKORN, R. A. 1983 *Flow Phenomena in Porous Media.* Dekker, New York.

GREENKORN, R. A., JOHNSON, C. R. & SHALLENBERGER, L. K. 1964 Directional permeability of heterogeneous anisotropic porous media. *Soc. Pet. Engrs J.* **4**, 124–132.

JOHNSON, W. E. & HUGHES, R. V. 1948 Directional permeability measurements and their significance. *Bull. mineral ind. exp. Stn. Penn St. Coll.* **52**, 180–205.

KUCUK, F. & BRIGHAM, W. E. 1979 Transient flow in elliptical systems. *Soc. Pet. Engrs J.* **267**, 401–410.

MARCUS, H. 1962 The permeability of a sample of an anisotropic porous medium. *J. geophys. Res.* **67**, 5215–5225.

NEALE, G. 1977 Degrees of anisotropy for fluid flow and diffusion (electrical conduction) through anisotropic porous media. *AIChE Jl* **23**, 56–62.

PATERSON, L. 1981 Radial fingering in a Hele Shaw cell. *J. Fluid Mech.* **113**, 513–529.

PINDER, G. F. & GRAY, W. G. 1977 *Finite Element Simulation in Surface and Subsurface Hydrology.* Academic Press, New York.

RICE, P. A., FONTUGNE, D. J., LATINI, R. G. & BARDUHN, A. J. 1970 Anisotropic permeability in porous media. *Ind. Engng Chem.* **62,** 23–31.

ROSE, W. D. 1982 A new method to measure directional permeability. *J. Pet. Technol.* **34,** 1142–1144.

SCHEIDEGGER, A. E. 1960 *The Physics of Flow Through Porous Media.* Macmillan, New York.

WHITAKER, S. 1970 Advances in theory of fluid motion in porous media. In *Flow Through Porous Media.* American Chemical Soc., Washington, D.C.

WILSON, D. G., SOLOMON, A. D. & BOGGS, P. T. (Eds) 1978 *Moving Boundary Problems.* Academic Press, New York.

WILSON, S. D. R. 1975 A note on the measurement of dynamic contact angles. *J. Colloid Interface Sci.* **51,** 532–534.